RSC Advances

ROYAL SOCIETY OF CHEMISTRY

www.rsc.org/advances

Novel Mononuclear Ruthenium(II) Complexes as Potent and Low-toxicity Antitumour Agents Synthesis, Characterization, Biological Evaluation and Mechanism of Action

Pengchao Hu,[a] Ying Wang,[a] Yan Zhang,[b] Hui Song,[c] Fangfang Gao,[a] Hongyi Lin,[a] Zhihao Wang,[a] Lei Wei*[a] and Fang Yang*[a]

[a] School of Basic Medical Sciences, Wuhan University, Donghu road No.185, Wuhan, China. E-mail: leiwei@whu.edu.cn

[b] School of Chemical and Biological Engineering, Tai Yuan Science and Technology University, Taiyuan, China

[c] Institute of Pathogen Biology, Chinese Academy of Medical Sciences and Peking Union Medical College, Beijing, China

Abstract: The ruthenium complex is considered a potential agent that could avoid the side-effects and chemoresistance of platinum-based anti-cancer drugs, such as cisplatin, carboplatin or oxaliplatin. In our study, three novel mononuclear ruthenium(II) complexes with salicylaldehyde as an ancillary ligand, $[Ru(bpy)_2(salH)]PF_6$ (**Ru-1**), $[Ru(dmb)_2(salH)]PF_6$ (**Ru-2**) and $[Ru(phen)_2(salH)]PF_6$ (**Ru-3**), where bpy = 2,2′-bipyridine, dmb = 4,4′-dimethyl-2,2′ bipyridine, phen = 1,10-phenanthroline, and salH = salicylaldehyde, have been synthesized, characterized and evaluated in vivo and in vitro. We showed that **Ru-2** effectively blocked DNA synthesis and induced cell apoptosis by interacting with double-stranded DNA. More significantly, **Ru-2** showed excellent antitumour effects in a cellular study (IC_{50} values of 3.60 μM for BGC823 human gastric cancer cells in vitro) and a xenograft model (inhibited tumour growth by 46%) at a dose of 5 mg/kg and exhibited insignificant hepatotoxicity and nephrotoxicity compared with a 4 mg/kg cis-platin-treatment. These results reveal that **Ru-2** might be a potential anticancer agent that could improve on the efficacy of common anticancer therapies, such as platinum-based drugs.

Introduction: Cancer is one of the major causes of death in the world. Currently, the clinical treatment of cancer is limited to surgery, radiotherapy, and chemotherapy. Although surgical resection and/or radiotherapy could cure early-stage solid tumours, most patients are diagnosed with advanced disease and distant metastases. In fact, chemotherapy appears to be the mainstay treatment for haematological and metastatic tumours[1]. However, common chemotherapeutic agents often have narrow therapeutic indices, due to their highly nonspecific cytotoxicity and undesirable side effects. Furthermore, their applications are limited by either intrinsic or acquired chemoresistance[2, 3]. More seriously, no curative therapy is available for most forms of disseminated cancer. From the therapeutic standpoint, the development of new compounds endowed with a specific anticancer activity is a burning issue [1, 4].

The successful development of new drugs must incorporate an extensive theoretical background, which includes the mechanism of action of these particular compounds. During recent decades, metal-based antitumour drugs have played a relevant role in antiblastic chemotherapy. For example, cisplatin is regarded as one of the most effective anticancer drugs in clinical treatment. Since the discovery of cisplatin by Rosenberg et al in 1964[5], research on metal-based drugs has become a challenging topic for in vivo and in vitro studies[6-8]. Although it is widely accepted that cisplatin is highly

effective against testicular, ovarian, bladder, and head and neck carcinomas[5, 9-12], platinum-based anti-cancer chemotherapy is associated with severe side effects because of its poor specificity[13, 14]. In the case of cisplatin, systemic toxicities, such as hepatotoxicity[15], nephrotoxicity[16, 17], neurotoxicity[18, 19], ototoxicity[17], and gametogenesis, inflict serious disorders or injuries[20, 21] and greatly restrict its efficacy. In addition, intrinsic and acquired drug resistances are key obstacles to the wider clinical application of platinum-based drugs[22-24]. The great success of cisplatin and these limitations have initiated efforts to develop new metal-based agents that will display improved therapeutic properties. In addition to the synthesis of new platinum complexes[25, 26] or drug modifications[27, 28], another approach is to examine complexes containing another transition metal.

Many transition metal complexes and small-molecule-based antitumour agents have been developed as new drugs[29-38]. Among the different metal complexes generating interest, ruthenium complexes have shown great potential and remain the subject of extensive drug discovery efforts because ruthenium has a low energy barrier between its oxidation states and a low atomic radius relative to the other transition metals in the series (0.125 nm), which are beneficial for its accumulation in cancer tissues[39, 40]. Recently, our group reported the use of some Ru(II) polypyridine complexes as antitumour agents were reported by our group[41, 42]. A large number of ruthenium (Ⅱ) complexes containing a $\{Ru(bpy)_2\}$(bpy = 2,2′-bipyridine) moiety with a variety of ancillary bidentate ligands have been reported[43-46]. One class of these ligands is the aldehyde ligands. These ligands are of particular interest because they play important roles in deciding the physical and chemical properties of the complex, due to the possibility of redox electron delocalization between the metal ion and the ligand[47-51].

In this study, three new ruthenium(II) complexes containing the ancillary ligand salicylaldehyde were synthesized and characterized using elemental analysis, IR, ^{1}H NMR spectroscopy and electrospray ionization mass spectrometry (ESI-MS). Moreover, these antitumour effects were investigated in vitro, and **Ru-2** exhibited the best inhibitory effect among three complexes. Furthermore, the anticancer and nonspecific effects of cisplatin and **Ru-2** were compared. The results showed that **Ru-2** could efficiently inhibit cancer growth in BGC823 cell xenografts and exhibited fewer side-effects, which indicates that **Ru-2** has enormous potenial as a novel chemotherapeutic drug.

Results and Discussion

Design and synthesis

All three complexes (Scheme 1) were synthesized using the general, previously reported method described below[52]: $AgNO_3$ (0.17 g, 1.0 mM) was added to ethanol solutions containing 0.5 mM $[Ru(bpy)_2Cl_2]\cdot 2H_2O$ (**Ru-1**), 0.5 mM $[Ru(dmb)_2Cl_2]\cdot 2H_2O$ (**Ru-2**) or 0.5 mM $[Ru(phen)_2Cl_2]\cdot 2H_2O$ (**Ru-3**), respectively. After refluxing for 30 min and filtering to remove the precipitated AgCl, the filtrate was added to an ethanol solution (30 ml) containing salicylaldehyde (52 μl, 0.5 mM) and NaOH (20 mg, 0.5 mM). The mixture was refluxed for 12 h under N_2. The resulting red solution was evaporated to dryness and the obtained solid was dissolved in water (15 ml). Excess KPF_6 was added to this water solution, a brown red solid was precipitated, and then solid crude $[Ru(bpy)_2(salH)]PF_6$ (**Ru-1**), $[Ru(dmb)_2(salH)]PF_6$ (**Ru-2**) and $[Ru(phen)_2(salH)]PF_6$ (**Ru-3**) residues were collected by filtration. To obtain the pure products, chromatographic purification was performed on a neutral aluminium oxide column, which afforded the complexes in good yields. The crystal structure of the **Ru-1** complex was reported in the literature[52] and was repeated in our experiments, while crystals of the **Ru-2** and **Ru-3** complexes were not obtained. However, ESI-MS and ^1H NMR helped us to determine their structure in solution.

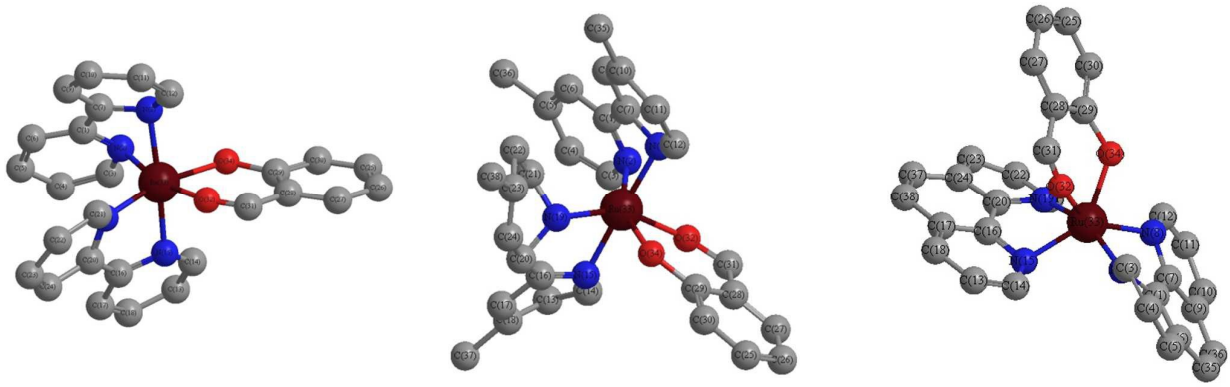

Ru-1 **Ru-2** **Ru-3**

Scheme 1. The structures of the complexes **Ru-1**, **Ru-2** and **Ru-3** with omitting the anion PF_6^-

In the ESI-MS of the **Ru-1**, **Ru-2** and **Ru-3** complexes, the peaks at m/z 535.0, 591.2 and 583.1 were designated to the species $[Ru(bpy)_2(salH)]^+$, $[Ru(dmb)_2(salH)]^+$ and $[Ru(phen)_2(salH)]^+$, respectively. A representative spectrum was shown in Fig. 1. The observed peaks revealed that the coordination cations of the three complexes were formed by one Ru(II) centre, one salH, and two bpy (or dmb, or phen) ligands, and the coordination cations were stable in the solution. The ^1H NMR spectra of the three

complexes were recorded in DMSO-d_6. The ^{1}H NMR spectrum of the **Ru-1** complex agreed with the literature[52]. The absence of the free SalH-OH proton (δ>10) in all spectra confirmed the complexation through the phenolate-O. The -CHO proton was observed in the range of 9.00-9.31 ppm. The aromatic region of each spectrum was very complicated because many of their aromatic hydrogen atoms had similar electronic environments, and their signals were shifted in a narrow range (7.2-8.8 ppm). The number of aromatic proton signals was consistent with the number of protons in the molecular formula; however, it is difficult to assign all of individual signals, respectively. In their solid state, the elemental analysis data agreed with the general formula including the PF_6^- anion.

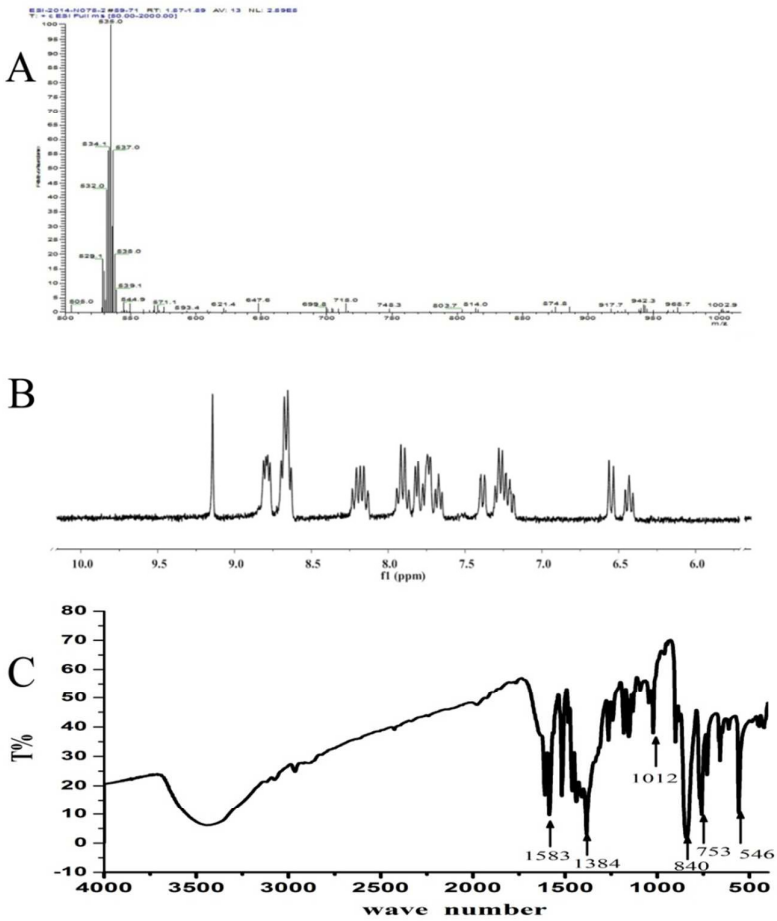

Fig. 1 Electrospray mass spectra in DMSO (A), ^{1}H NMR spectrum in DMSO-d_6 (B) and infrared spectra of a KBrpellet (C) of the **Ru-1** complex in a dimethyl sulfoxide (DMSO) solution.

Photophysical and electrochemical properties

The infrared spectra of the complexes did not display any band near 3300 cm^{-1}, which suggested that the

phenolate-OH of salH was deprotonated in the complexes. The free aldehydes displayed a peak near 1650 cm^{-1} that was assigned to the C=O group. A medium to strong peak was observed in the range 1590-1640 cm^{-1} for all the three complexes. This peak might originated from the metal-coordinated C=O group of salH. The strong and sharp peaks displayed by the complexes from 1570-1590 cm^{-1} were likely to be associated with the C=N fragments of the ancillary ligands. The presence of PF_6^- in each complex was indicated by a strong peak at 840 cm^{-1}[52].

The absorption spectra of the three complexes were recorded in acetonitrile (Fig. 2).With the exeption of **Ru-3**, the spectral profiles of the other complexes were very similar. **Ru-1** and **Ru-2** displayed three absorptions peaks at 490-495 nm, 355-365 nm and 287-295 nm, **Ru-3** displayed two absorptions peaks at 430-440 nm and 260-265 nm. These absorption peaks for **Ru-3** were significantly blue shifted compared with the other complexes. The bands at 260, 290 and 360 nm are attributed to intraligand $\pi\rightarrow\pi^*$ transitions. The lowest energy bands, approximately 430 and 490 nm, are assigned to metal-ligand charge transfer (MLCT) ($d_{Ru}\rightarrow\pi^*$)[53]. Excitation of the Ru-complexes at 450 nm resulted in single emission peak at 595 nm for **Ru-1**, 593 nm for **Ru-2** and 584 nm for **Ru-3**. The spectral data of the **Ru-1, Ru-2** and **Ru-3** complexes in acetonitrile solutions were listed in Table 1.

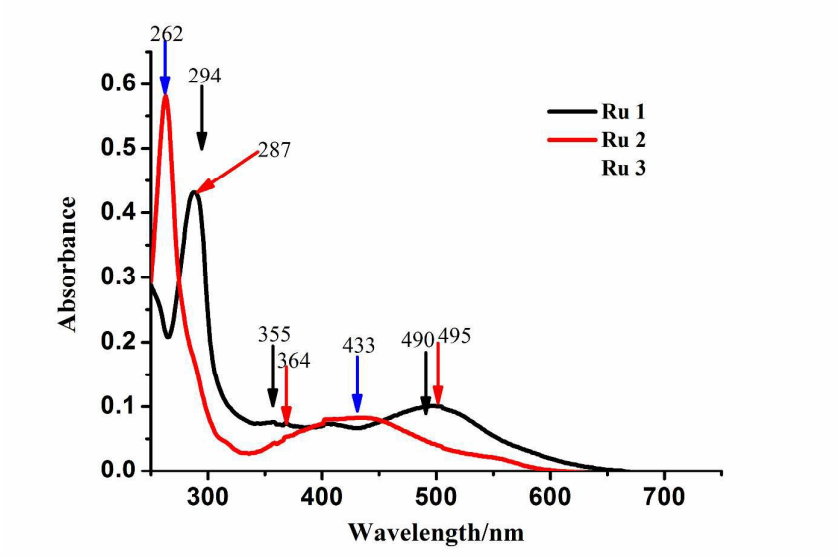

Fig. 2 The absorption spectrum of **Ru-1**, **Ru-2** and **Ru-3** in acetontrile solution.

Table 1. The Spectral Characteristics of Ru-complexes in degassed acetonitrile

a absorption spectroscopic data

Complexes	λ_{max}/nm ($\varepsilon\times10^{-3}$/$dm^3\cdot mol^{-1}\cdot cm^{-1}$)	
	$\pi\leftarrow\pi^*/\pi\leftarrow n$	MLCT

Ru-1	294(48.16),355(8.72)	490(8.43)
Ru-2	287(43.18),364(6.95)	495(10.45)
Ru-3	262(57.51)	433(8.11)

b emission spectroscopic data

Complexes	λ_{ex}/nm	λ_{max}^{em}/nm
Ru-1	452	595
Ru-2	453	593
Ru-3	452	584

Acetonitrile solutions of all the complexes were used to study the redox behaviour using cyclic voltammetry. Representative voltammograms were shown in Fig. 3 and the potential data are provided in Table 2. The complexes displayed the Ru^{III}/Ru^{II} couple at potentials ranging from 0.60-1.02 V (*vs. SCE*). The one electron stoichiometry of this response was confirmed for each complex by comparing the peak currents with known one electron redox processes under identical conditions[54, 55].

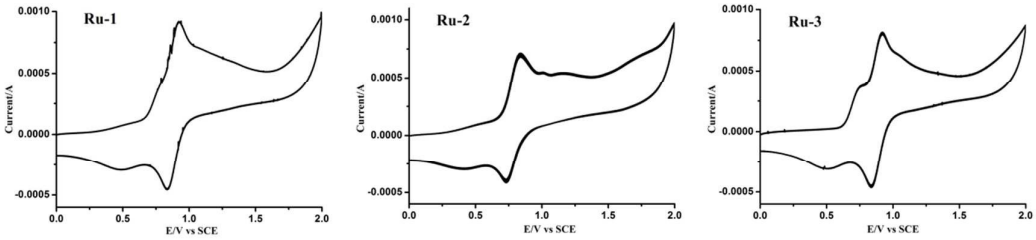

Fig. 3 Cyclic voltammograms of **Ru-1**, **Ru-2** and **Ru-3** were carried out in CH_3CN solution with Bu_4NClO_4 (0.1 M). (Scan rate 100 mV/s)

Table 2. Cyclic voltammetric data in degassed acetonitrile at 298 K

Complexes	E_{pa}(V)	E_{pc}(V)	$E_{1/2}$(V)	ΔE_p(mV)
Ru-1	0.834	0.939	0.886	105
Ru-2	0.731	0.841	0.786	110
Ru-3	0.826	0.904	0.865	78

Biological results

Ru-complexes reduced cell viability and proliferation. The A549 (human bronchogenic carcinoma cell line), BGC823 (human gastric cancer cell line) and MDA-MB-231 (human breast cancer cell line) cells were treated with different concentrations of **Ru-1**, **Ru-2** and **Ru-3** for 24 h and 48 h. The cytotoxicity of these complexes towards the aforementioned cell lines was evaluated using the MTT method. Culture medium containing 0.05% DMSO was used as the negative control. The IC_{50} values were listed in Table 3,

and the cell viabilities were shown in Fig. 4. The cell viability was obviously decreased as the concentration and incubation time increased. As shown in Table 3, it was clear that **Ru-2** was generally the most active complex and exhibited low IC_{50} values, particularly at the concentrations of 7.97 and 3.60 μM for the A549 and BGC823 cells, respectively, at 48 h. The cytotoxicity of **Ru-1** was higher than that of **Ru-3** towards A549 and BGC823 cells, and there was an opposite phenomenon in the MDA-MB-231 cells, but these IC_{50} values were obviously higher than those of **Ru-2** in all three cell lines. Overall, among these complexes, **Ru-2** exhibited the highest cytotoxicity in A549, BGC823 and MDA-MB-231 cells. Furthermore, the colony formation assay revealed that the malignant cells generated fewer colonies as the concentration of the Ru-complexes increased. Representative pictures are shown in Fig. 5. Following treatment with the Ru-complexes, the colony number was significantly decreased and the size of a single colony was reduced, with the exception of the MDA-MB-231 cells that were treated with 10 μM **Ru-1**. Similar to the cytotoxicity study, **Ru-2** showed the strongest inhibitory effect, as the number of A549 and BGC823 colonies was nearly zero after treatment with 5 μM **Ru-2**. The activity of anticancer drugs is often related to their lipophilic character, such that the resulting hydrophobicity may contribute to an increased uptake of the complex by the cells, thereby enhancing the antiproliferative activity. The differences in the cytotoxicity of these complexes may be caused by the different ancillary ligands. These results clearly indicate that structural changes in the ancillary ligands have an important impact on the cytotoxicity in vitro.

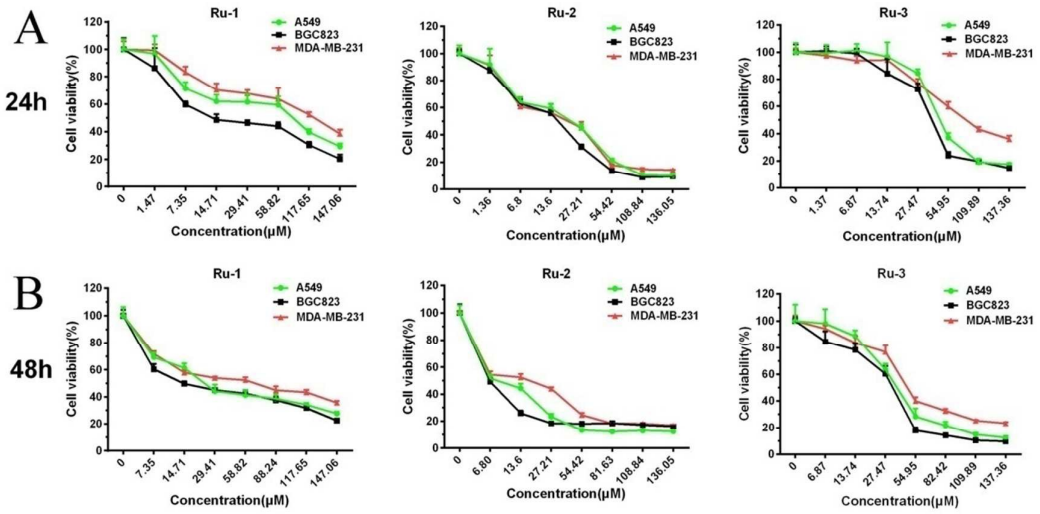

Fig. 4 The Ru-complexes inhibited cell viability. (A) The A549, BGC823, and MDA-MB-231 cells were treated with **Ru-1**, **Ru-2**, and **Ru-3** (1-150 μM) for 24 h. (B) A549, BGC823, and MDA-MB-231 cells were treated with **Ru-1**, **Ru-2**, and **Ru-3** (5-150 μM) for 48 h. Cell viability was measured with the MTT assay. Data from three independent experiments run in sextuplicate are shown.

Table 3. IC_{50} Values of Ru-complexes against Human Tumour cell lines

time	complexes	IC_{50}(μM) [a]		
		A549	BGC823	MDA-MB-231
24h	**Ru-1**	55.26±2.4	20.58±0.73	101.50±3.06
	Ru-2	16.88±0.68	12.85±1.12	15.52±1.23
	Ru-3	50.70±1.23	39.12±1,52	82.82±2.61
	CDDP [b]	28.59±0.94	4.46±0.22	22.46±1.62
48h	**Ru-1**	29.7±2.22	18.75±0,42	50.62±1.66
	Ru-2	7.97±0.19	3.60±0.06	12.47±0.69
	Ru-3	37.65±1.78	29.39±0.42	59.21±1.45

[a] Concentration of compounds that inhibit 50% human tumour cell growth, presented as the mean±SD and performed in sextuplicate.

[b] Culture medium containing cis-Dichlorodiammineplatinum(II) (CDDP) was used as the positive control, the cell viabilities were shown in Fig. 9A.

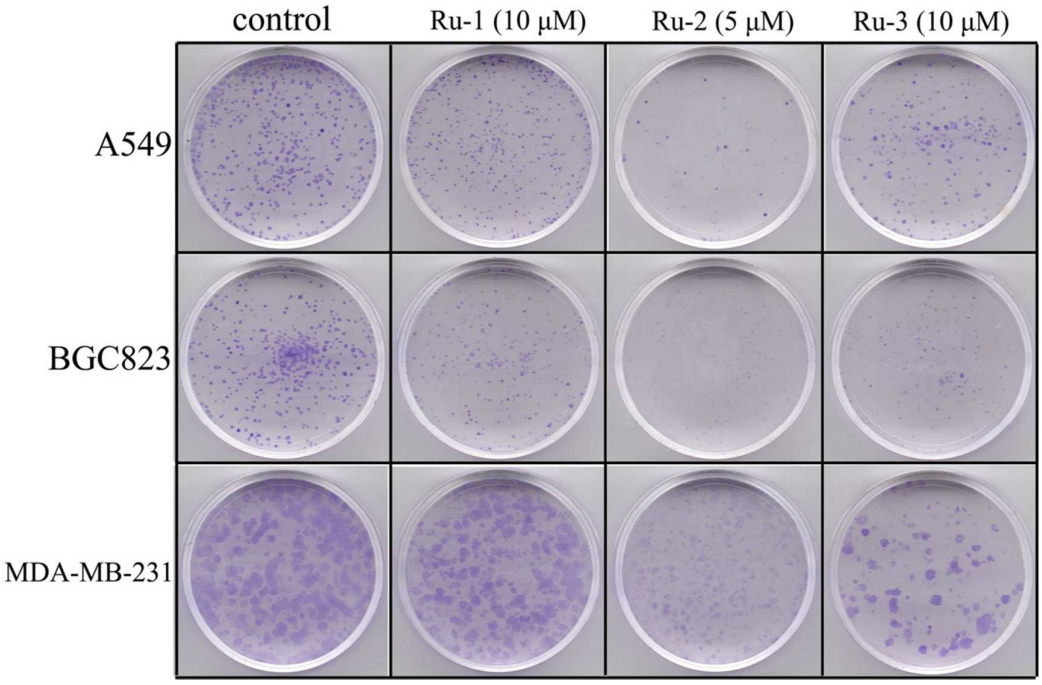

Fig. 5 The Ru-complexes inhibit cell proliferation and induce cancer cell death. Colony formation assays were used to measure the clonogenicity of cancer cells after treatment with the Ru-complexes. A549, BGC823, and MDA-MB-231 cells were seeded in 35 mm culture dish and incubated with 10 μM **Ru-1**, 5 μM **Ru-2**, and 10 μM **Ru- 3** for 2 weeks. Culture medium containing 0.5% (V/V) DMSO was used as the control group.

The Ru-complexes could effectively induce cancer cell apoptosis. Hoechst 33258 is a membrane permeable dye that stains the nucleus. Live cells with uniformly light blue nuclei are observed under a fluorescence microscope, apoptotic cells have bright blue nuclei due to karyopyknosis and chromatin condensation, and the nuclei of dead cells cannot be stained[56]. To observe the morphological characteristic of apoptotic nuclei, the A549, BGC823 and MDA-MB-231 cells were stained with Hoechst 33258 after exposure to 10, 20 and 40 μM **Ru-1** and **Ru-3** or 5, 10 and 20 μM **Ru-2** and were assayed with a Laser scanning confocal microscope. The cells that had been treated with 0.05% (v/v) DMSO were used as the negative control. Representative images are shown in Fig. 6. The control cells displayed a regular circle shape and homogeneous nuclear staining. After treatment with the Ru-complexes, the number of stained nuclei representing the surviving cells decreased as the concentrations of the Ru-complexes increased, and the number of apoptotic cells increased in a dose-dependent manner and exhibited typical apoptotic features, such as bright staining, condensed chromatin, and fragmented nuclei. These results show that the Ru-complexes can effectively induce cancer cell apoptosis.

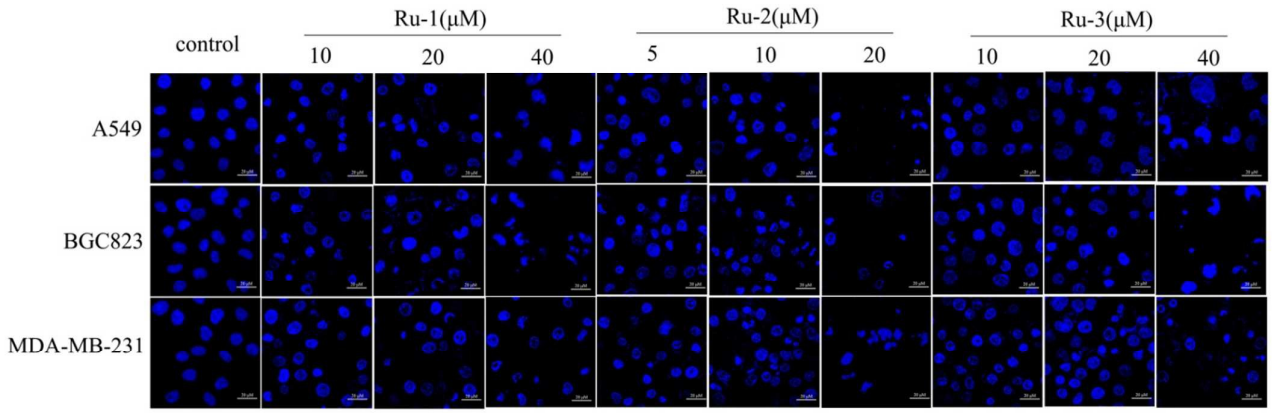

Fig. 6 Changes in the nuclear morphology cancer cells that were treated with the Ru-complexes for 24 h. The cells were seeded in 24-well plates and treated with **Ru-1**, **Ru-3** (10, 20, 40 μM), and **Ru-2** (5, 10, 20 μM) for 24 h. Then, the cells were stained with Hoechst 33258 and observed under a confocal microscope. Original magnification × 600.

The Ru-complexes inhibited DNA amplification in cancer cells. Metal-containing compounds, such as platinum and ruthenium drugs, induce programmed cell death by blocking DNA synthesis[1]. Thus, in this study, we performed the EdU incorporation assay, a sensitive and specific method, to compare the effects of the Ru-complexes on DNA synthesis and cell proliferation. EdU can be incorporated into the synthesizing DNA molecules in place of thymine; thus, cells in S phase can be stained and exhibit fluorescence[57]. As shown in Fig. 7, the number of EdU^+ cells (EdU-labelled replicating cells) was gradually reduced after treatment with increasing concentrations of the Ru-complexes. More importantly, compared with the control group, the number of Hoechst-stained cells (surviving cells) was also significantly decreased. Overall, the Ru-complexes efficiently inhibit DNA synthesis and cell proliferation, particularly **Ru-2**.

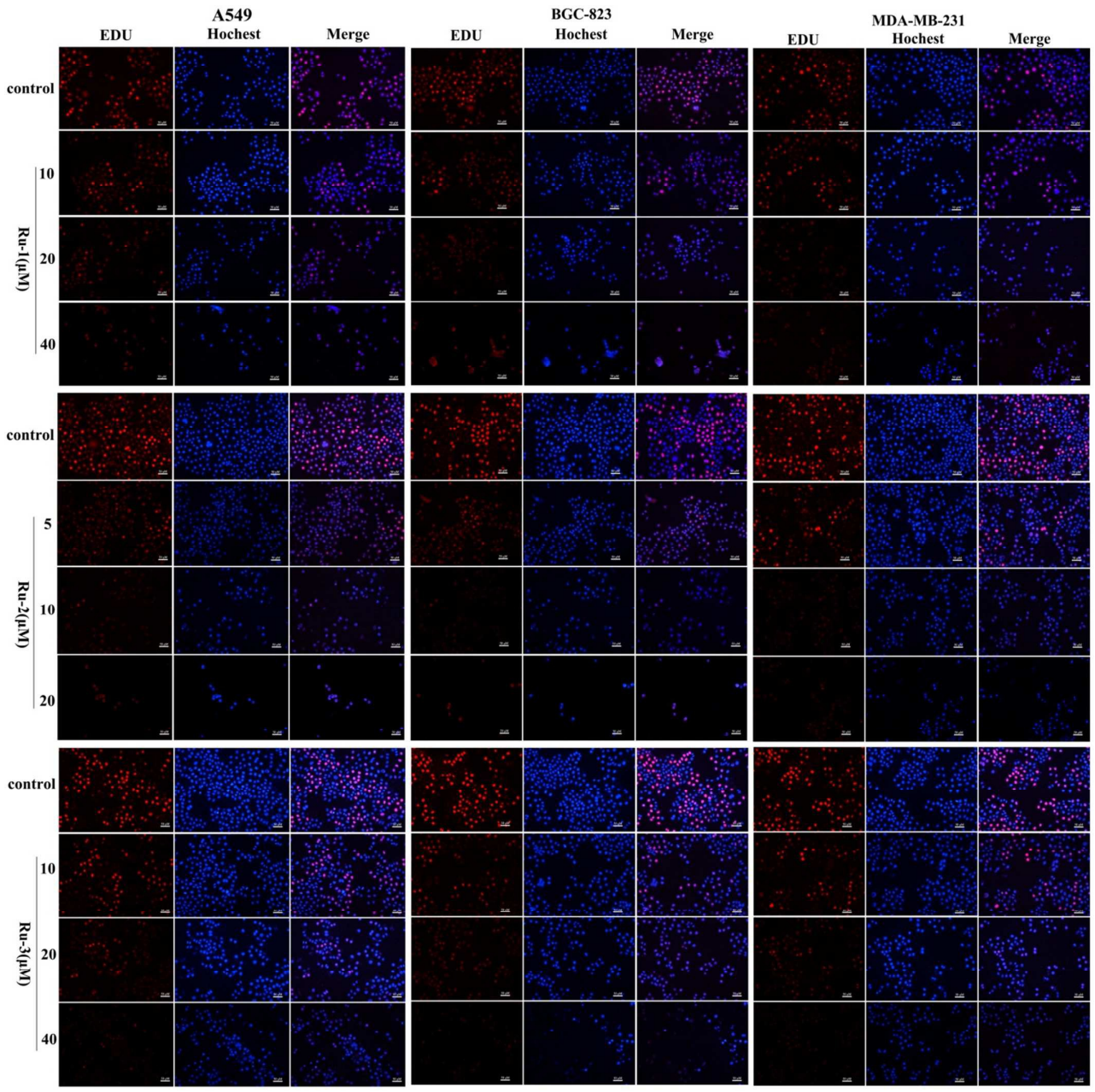

Fig. 7 Ru-complexes inhibit DNA amplification and cell proliferation. EdU staining was used to detect the efficiency of DNA amplification in cancer cells after treatment with the Ru-complexes. The cells were seeded in 12-well plates and treated with **Ru-1**, **Ru-3** (10, 20, 40 μM), and **Ru-2** (5, 10, 20 μM) for 24 h. Then, the cells were analysed with fluorescent inverted microscope as described in the Experimental Section. Original magnification × 200.

DNA binding studies: emission titrations. The antitumour activity of metal-containing agents is generally accepted to involve binding to DNA. Intracellular interaction with DNA is likely to be of central importance in explaining their toxicity towards rapidly dividing tumour cells[1]. Therefore, the DNA

binding properties of the Ru-complexes were probed by monitoring the changes in their fluorescence emission spectra in the presence or absence of DNA [58, 59]. The fluorescence measurements were also performed to clarify the interaction mode between the complexes and DNA.

The maximum emission wavelength of approximately 600 nm appeared when the Ru-complexes were excited at 450 nm in Tris-Cl buffer (10^{-4} M, pH 7.4). Fig. 8 illustrated the changes in fluorescence of **Ru-1/2/3**by the titration of various concentrations of CT-DNA. Upon addition of DNA, **Ru-2** exhibited significant quenching, and the maximal quenching reached 71%. However, the fluorescence quenching of **Ru-1** and **Ru-2** was obviously reduced, and was only 11% for **Ru-1** and 18% for **Ru-3**. The observed fluorescence quenching of the complexes by CT-DNA is consistent with a photoelectron transfer from the guanine base of DNA to the excited MLCT state of the Ru(II) complex as reported for $[Ru(TAP)_3]^{2+}$, $[Ru(bzimpy)_2]^{2+}$, and $[Ru(bpz)_3]^{2+}$ [bzimpy-bis(N-alkylbenzimidazol-2'-yl)pyridines]; TAP = 1,4,5,8-tetra-aza-phenanthrene; bpz = 4,4'-bipyrazole[60-62]. In addition, it was found that the groove binding interaction between naproxen and double stranded-DNA (ds-DNA) caused a strong fluorescence quenching[63, 64]. This decrease in the emission intensity of the complexes also agreed with the findings obtained using other non-intercalators[65, 66]. The quenching constants (*Ksv*) were calculated using the Stern-Volmer fluorescence quenching equation, $F_0/F=1+Ksv[Q]$, where F_0 and F are the fluorescence intensities in the absence and presence of a quencher, respectively[67]. The quenching constants were calculated to be 0.66×10^4, 0.355×10^5 and 0.67×10^4 mol/L for **Ru-1**, **Ru-2** and **Ru-3**, respectively. These results reveal that the interaction between **Ru-1/2/3 and** ds-DNA is consistent with the groove binding mode, and **Ru-2** binds more strongly compared with **Ru-1** and **Ru-2**, which is consistent with the cytotoxicity study.

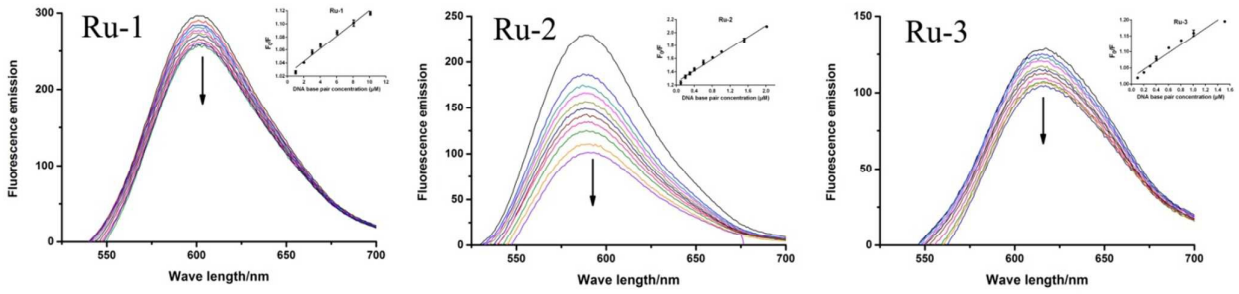

Fig. 8 The fluorescence emission (λ ex = 450 nm) of the Ru-complexes decreases upon titration with CT-DNA. (A) Approxomately 19.6 μM **Ru-1**, (B) 18.1 μM **Ru-2**, (C) 18.3 μM **Ru-3** were dissolved in Tris-Cl buffer (10^{-4} M, pH7.4), and titrated with CT-DNA (0, 1.01, 2.02, 3.03, 4.04, 6.06, 8.08, 10.1, 15.2, 20.2 and 30.3 μM).

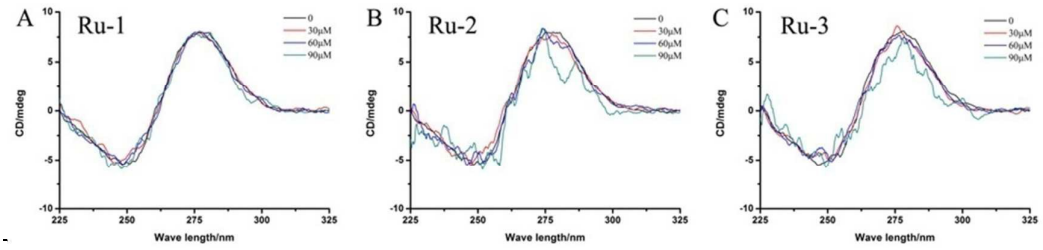

Comparison of the anti-cancer effects of CDDP and Ru-2 in vitro. From the above results, it was clear that **Ru-2** showed the highest cytotoxicity and the strongest DNA binding ability among the three complexes. Consequently, **Ru-2** was selected for a comparison with cis-Dichlorodiammineplatinum(II) (CDDP), one of the most common clinical platinum–based drugs. The A549, BGC823 and MDA-MB-231 cells were treated with different concentrations of CDDP and **Ru-2** for 24 h and cytotoxicity was evaluated by the MTT method. As shown in Fig. 9A, the results showed that **Ru-2** was more active than CDDP in the A549 and MDA-MB-231 cell lines, but bot the BGC823 cell line, and exhibited lower IC_{50} values of 13.19 μM and 11.63 μM for the A549 and MDA-MB-231 cells, respectively, compared with those of CDDP, 28.59 and 22.46 μM, respectively. For the BGC823, the IC_{50} values were 9.21 μM for **Ru-2** and 4.46 μM for CDDP. More interestingly, we found that the Ru-2-induced cytotoxicity exhibited a better linear dependence on concentration. Next, the colony formation assay was performed to evaluate the long-term survival of BGC823 treated with CDDP and **Ru-2**. As shown in Fig. 9B, the colony number of the cells that were exposed to 0.5 μM CDDP and **Ru-2**, was approximately half that of the control group. When the concentration reached 5 μM, the colony number was nearly zero. Then, the dissipation of the mitochondrial membrane potential (ΔΨm) was assessed by JC-1 staining, which reveals the status of mitochondria, and the loss of ΔΨm is usually deemed as a characteristic of early apoptosis. BGC823 cells were treated with **Ru-2** and CDDP. Representative images were shown in Fig. 9C. In the control group, the JC-1 staining mostly aggregated in the mitochondria and the ratio of JC-1 polymer/monomer was approximately 3.15. After treatment with CDDP and **Ru-2**, the red fluorescence obviously decreased, and the green fluorescence significantly increased, the ratio reduced to 0.95, which indicated the dissipation of ΔΨm and the occurrence of apoptosis. To determine the percentage of apoptotic cells, apoptosis was investigated by flow cytometry.

After incubation with CDDP and **Ru-2** for 24 h, the proportions of apoptotic and necrotic BGC823 cells were significantly increased compared with the control group (Fig. 9D).

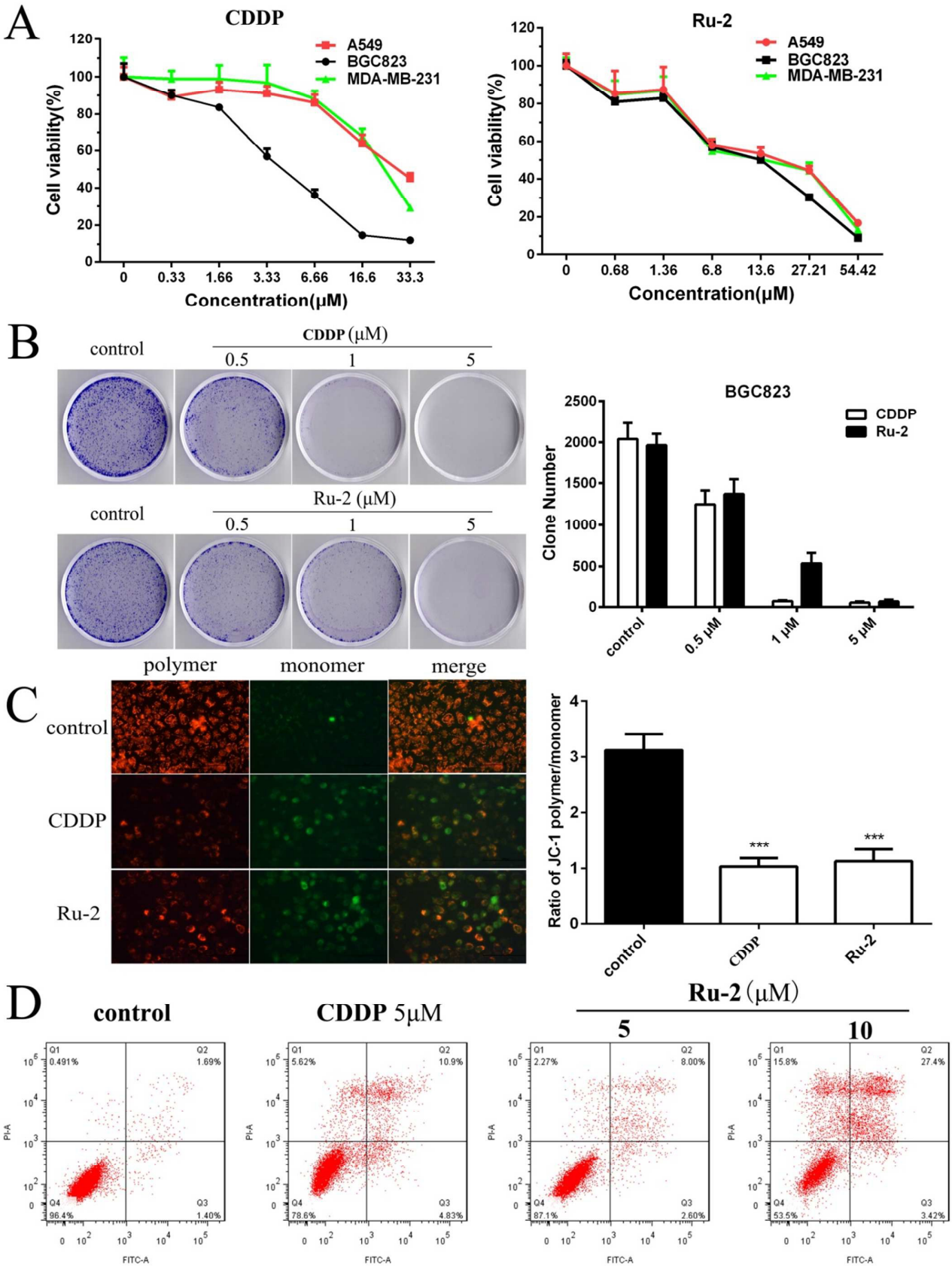

Fig. 9 Comparison of the anti-cancer effects of Ru-2 and CDDP in vitro. (A) The MTT assay was used to measure

cell viability after treatment with **Ru-2** (0-55 μM) and CDDP (0-35 μM). **(B)** The colony formation assay was used to measure the clonogenicity of BGC823 cells that had been treated with 0.5, 1, 5 μM CDDP and **Ru-2**. **(C)** BGC823 was incubated with 5 μM CDDP and **Ru-2** for 12 h, and then the dissipation of mitochondrial membrane potential (ΔΨm) was assessed by JC-1 staining. **(D)** The percentage of live, and apoptotic BGC823 cells was detected and analysed by flow cytometry.

Ru-2 corrects the metabolic disorder and inhibits cancer growth in vivo. Given the dramatic differences in the physiology of cancer cells grown in culture and cancer cells in vivo, we assessed the antitumour potential of **Ru-2** in BGC823 cell xenografts. Subcutaneous tumours were allowed to grow to ~100 mm^3 and then mice were intraperitoneally injected with **Ru-2** (5 mg/kg), CDDP (4 mg/kg) or vehicle (normal saline) every other day for 30 days. We did not observe a significant change in body weight until the tumours were ~400 mm^3. At this point, the tumours exhibited rapid growth and produced a dramatic decrease in body weight due to the negative energy balance. As shown in Fig. 10, there was an obvious and slow change in both the body weight loss and the growth of the subcutaneous tumours when the animals were treated with CDDP or **Ru-2**, and tumour outgrowth was significantly reduced. Indeed, the tumours from the CDDP- or **Ru-2**-treated animals were approximately half the size of the control group at the time of sacrifice. The tumour weights were reduced by 40% following CDDP treatment, and by 46% following **Ru-2** treatment. Taken together, these results show that **Ru-2** is capable of correcting the metabolic disorder and inhibiting cancer growth to some extent.

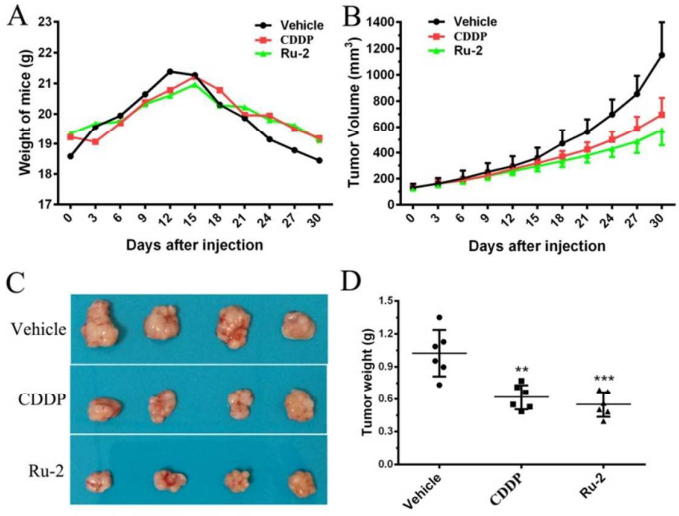

Fig. 10 Ru-2 suppresses BGC823 xenograft growth in vivo. BGC823 cells were subcutaneously injected into 6-7-week-olds nude mice and randomly distributed into three groups (n=6) that were intraperitoneally injected with the vehicle only (normal saline), 4 mg/kg body weight CDDP, or 5 mg/kg of body weight **Ru-2** for 30 days. **(A)** The body weights of the mice were recorded at the indicated time after the injection of vehicle, CDDP and **Ru-2**. **(B)** **The**

tumour volumes were measured by calipers every 3 days. **(C)** Representative xenograft tumours from mice treated with vehicle, CDDP and **Ru-2** were shown. **(D)** The weights of the tumours from the nude mice were measured and a statistical analysis was conducted. The symbol "**" indicates $P < 0.01$ vs the vehicle group, and "***" indicates $P < 0.001$.

Ru-2 exhibited lower hepatotoxicity and nephrotoxicity than CDDP. Based on the systemic toxicities of cisplatin, such as hepatotoxicity and nephrotoxicity, we assessed the liver and kidney damage caused by **Ru-2**. We found that the livers derived from the mice injected with CDDP showed visual hepatomegaly compared with the vehicle-treated animals, and the livers from the **Ru-2**-treated animals fell between the two. This result was confirmed by the follow-up experiment. The livers from the CDDP-treated animals showed the largest weights among the three groups, and those from the **Ru-2**-treated animals were the second heaviest (Fig. 11A). The serum alanine aminotransferase (ALT) and aspartate aminotransferase (AST) activities can indicate normal (liver) cell toxicity in vivo[68]. We further tested the serum ALT and AST levels in nude mice following with the vehicle, CDDP and **Ru-2** treatments, and found that the serum ALT and AST levels in the CDDP- and **Ru-2**-treated mice were clearly increased compared with the vehicle-treated mice (Fig. 11C and 11D). **Ru-2** treatment led to an approximately 1.5-fold increase in the ALT and AST levels compared with the vehicle-treated mice. However, CDDP resulted in an approximately 2.5-fold increase. Furthermore, the liver and kidney tissues were subjected to a pathological analysis. As shown in Fig. 11E, the vehicle-treated group showed a normal histology by H&E staining. The light microscopy analysis revealed that the liver sections from the CDDP-treated nude mice, displayed many pathological alterations, such as hepatocyte swelling, bile duct proliferation and partial inflammatory cell infiltration. Moreover, we found that the cytoplasm of some hepatocytes was light, foamy, and filled with numerous vacuoles, the cellular outlines were vague, and the hepatic cord was disordered. These results are consistent with CDDP-induced pathological changes in liver that were reported previously[15, 69]. In the liver sections from the **Ru-2**-treated nude mice, there was a very slight crisis compared with the CDDP-treated mice, and the liver parenchyma was comparable with that of the vehicle-treated group to some extent, except that it exhibited a slightly blurred trabecular structure, and partial cytoplasmic vacuolization. All of these histological abnormalities coincided with the increased ALT and AST activities. Furthermore, histological abnormalities were observed in kidney sections from the CDDP- or **Ru-2**-treated mice, although there was no observable difference in the weights of the kidneys (Fig. 11B). The histopathological changes induced by CDDP included renal

tubular necrosis, detachment of the cellular content, nucleus karyolysis, glomerular shrinkage, Bowman's space expansion and an incomplete renal capsule wall layer. However, the kidneys from the **Ru-2** group were fairly comparable to the vehicle-treated group, except for a slightly expanded Bowman's space and glomerular shrinkage (Fig. 11E). These results suggest that **Ru-2** exhibits excellent anticancer activity with few side effects.

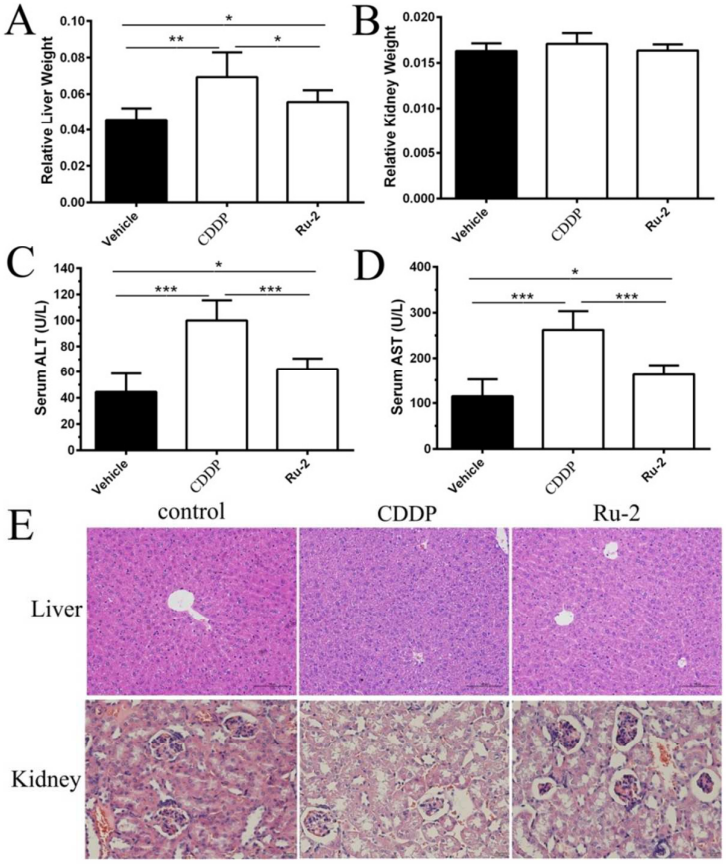

Fig. 11 The injury of liver and kidney induced by CDDP and Ru-2. (A) The weight of livers derived from BGC823 xenograft nude mice was measured, and relative liver weight indicated the ratio of liver weight to body weight. **(B)** Relative liver weights were calculated and there was no significant difference among three groups. The serum ALT **(C)** and AST **(D)** activities were detected from the indicated nude mice. **(E)** The H&E staining revealed hepatotoxicity and nephrotoxicity in histological appearance in nude mice treated with vehicle, CDDP and **Ru-2**. The symbol "*" indicates $P < 0.05$, "**" indicates $P < 0.01$, and "***" indicates $P < 0.001$.

Conclusions

In this study, three mononuclear ruthenium complexes (**Ru-1**, **Ru-2** and **Ru-3**) were designed, efficiently synthesized, and evaluated in vitro and in vivo. The most potent compound, **Ru-2**, showed excellent DNA

binding activity in the DNA titration assay, with quenching constants of 0.355×10^5 mol/L, and significant antiproliferative ability in the cellular study, with IC_{50} values of 3.60 μM for the BGC823 cells. As a probe in the mechanism studies, **Ru-2** blocked DNA amplification in cancer cells and induced apoptosis, thus inhibiting the tumour growth of BGC823 cell xenografts. After assessing the drug-like properties of the three Ru-complexes, **Ru-2** and CDDP were evaluated in parallel to determine their antitumour activity and systemic toxicities in vitro and in vivo. **Ru-2** displayed less toxicity to normal cell types and excellently suppressed tumour growth by 46% at a dose of 5 mg/kg. It was more exciting that **Ru-2** exhibited insignificant hepatotoxicity and nephrotoxicity compared with CDDP, which induced visual hepatomegaly, a clear increase in the serum ALT and AST levels, and pathological morphological disordersin the liver and kidney tissues. All of these data reveal that **Ru-2** might be a potential anticancer agent with no obvious signs of toxicity, and it could replace the conventional platinum-based antitumour drugs.

Experimental Section

Chemistry. Materials and Methods. All reagents and solvents were of commercial origin and were used without further purification unless otherwise noted. Ultrapure Milli-Q water was used in all experiments. $RuCl_3\cdot3H_2O$, 2,2′-bipyridyl(bpy), 4,4′-dimethyl-2,2′ bipyridine(dmb), 1,10-phenanthroline(phen), and salicylaldehyde(salH) were purchased from Wuhan Shenshi Huagong, and the $Ru(R)_2Cl_2\cdot2H_2O$(R = bpy, dmb and phen) were synthesized and purified according to published methods[61]. Microanalysis (C, H, and N) was conducted with a PerkinElmer 240Q elemental analyser. The electrospray ionization mass spectra were recorded with an LCQ system (Finnigan MAT, USA) using CH_3OH as the mobile phase. The 300 MHz ^1H NMR spectroscopic measurements were performed on a Bruker AM-300 NMR spectrometer, using DMSO-d_6 as solvent and TMS ($SiMe_4$) as an internal reference at 25 °C. The infrared spectra were recorded on a Perkin-Elmer Spectrum FT-IR spectrometer using KBr pellets. The solution electronic absorption and emission spectra were recorded in acetonitrile on a Shimadzu 3100 spectrophotometer and a Shimadzu RF-5301 PC spectrofluorometer, respectively. Cyclic voltammetry (CV) was performed with a CHI 630E instrument in a three-electrode cell with a pure Ar gas inlet and outlet. The working electrode and counter electrode were Pt electrodes, and the reference electrode was a saturated calomel electrode (*SCE*). The experiments were performed out in the presence of CH_3CN. The CV experiments were

performed with a scan rate of 100 $mV \cdot s^{-1}$.

General Procedure for the purification and identification of Ru-complexes.

All three complexes were synthesized using a general, previously reported method[52].

[Ru(bpy)$_2$(salH)]PF$_6$ **(Ru-1)**: $AgNO_3$ (0.17 g, 1.0 mM) was added to an ethanol solution of $[Ru(bpy)_2Cl_2]\cdot 2H_2O$(0.26 g, 0.5 mM). After refluxing for 30 min and filtering to remove the precipitated AgCl, the filtrate was added to an ethanol solution (30 ml) of salicylaldehyde (52 μl, 0.5 mM) and NaOH (20 mg, 0.5 mM). The mixture was refluxed for 12 h under N_2. The resulting red solution was evaporated to dryness and the obtained solid was dissolved in water (15 ml). To this water solution, excess KPF_6 was added, a brown red solid was precipitated, and then solid crude $[Ru(bpy)_2(salH)]PF_6$ residues were obtained. The crude residue was washed thoroughly with water and dried in vacuum over P_2O_5. The complex was purified on a neutral aluminium oxide column. The first moving brown red band was eluted with dichloromethane containing 5% acetone, and then the solids were collected and evaporated[48]. Yield: 0.46 g, 68%. Anal. Calcd (%) for $C_{27}H_{21}N_4O_2PF_6Ru$: C, 47.72; H, 3.11; N, 8.25. Found(%): C, 47.73; H, 3.11; N, 8.27. ^{1}H NMR (300 MHz, DMSO-d_6)[ppm]:6.53(1H, d, J=9.0 Hz), 7.21(1H, d, J=6.0 Hz), 7.26(2H, d, J=6.0 Hz), 7.37(1H, d, J=9.0 Hz), 7.67(1H, m), 7.73(2H, d, J=3.0 Hz), 7.80(2H, m), 7.89(2H, d, J=9.0 Hz), 8.16-8.23(2H, m), 8.63-8.70 (4H, m), 8.78(2H, m), 9.14(1H, s). IR (KBr) [cm^{-1}]:1608, 1583, 1505, 1427, 1384, 1254, 1142, 1012, 840, 753, 658, 546. ESI-MS(DMSO): m/z 535.0 ($[Ru(bpy)_2(salH)]^+$).

[Ru(dmb)$_2$(salH)]PF$_6$ **(Ru-2)**: $AgNO_3$ (0.17 g, 1.0 mM) was added to an ethanol solution of $[Ru(dmb)_2Cl_2]\cdot 2H_2O$(0.29 g, 0.5 mM). After refluxing for 30 min and filtering to remove the precipitated AgCl, the filtrate was added to an ethanol solution (30 ml) of salicylaldehyde (52 μl, 0.5 mM) and NaOH (20 mg, 0.5 mM). The mixture was refluxed for 12 h under N_2. The resulting red solution was evaporated to dryness and the obtained solid was dissolved in water (15 ml). To this water solution, excess KPF_6 was added, a brown red solid was precipitated, and then solid crude $[Ru(dmb)_2(salH)]PF_6$ residues were obtained. The crude residue was purified as the procedure similar to that described for complex **Ru-1**. Yield: 0.53 g, 72%. Anal. Calcd (%) for $C_{31}H_{29}N_4O_2PF_6Ru$: C, 50.61; H, 3.97; N, 7.62. Found(%): C, 50.59; H, 3.99; N, 7.61. ^{1}H NMR (300 MHz, DMSO-d_6)[ppm]:2.43(6H, s), 2.54(6H, s), 7.06(1H, d, J=6.0 Hz), 7.24(1H, m), 7.32-7.36 (2H, m), 7.48-7.54(2H, m), 7.59(2H, m), 7.70(1H, d, J=3.0 Hz), 7.93(1H, d, J=6.0 Hz), 8.46(2H, m), 8.64-8.7(4H, m), 9.13(1H, s). IR (KBr) [cm^{-1}]: 1621, 1573, 1506, 1467, 1381, 1237, 1142, 1083, 1016, 882, 824, 747, 727, 651, 546. ESI-MS(DMSO): m/z 591.2 ($[Ru(dmb)_2(salH)]^+$).

[Ru(phen)$_2$(salH)]PF$_6$ **(Ru-3)**: $AgNO_3$ (0.17 g, 1.0 mM) was added to an ethanol solution of $[Ru(phen)_2Cl_2]\cdot 2H_2O$(0.28 g, 0.5 mM). After refluxing for 30 min and filtering to remove the precipitated AgCl, the filtrate was added to an ethanol solution (30 ml) of salicylaldehyde (52 μl, 0.5 mM) and NaOH (20 mg, 0.5 mM). The mixture was refluxed for 12 h under N_2. The resulting red solution was evaporated to dryness and the obtained solid was dissolved in water (15 ml). To this water solution, excess KPF_6 was added, a brown red solid was precipitated, and then solid crude $[Ru(phen)_2(salH)]PF_6$ residues were obtained. The crude residue was purified as the procedure similar to that described for complex **Ru-1**. Yield: 0.49g, 67%. Anal. Calcd (%) for $C_{31}H_{21}N_4O_2PF_6Ru$: C, 51.18; H, 2.91; N, 7.70. Found(%): C, 51.20; H, 2.91; N, 7.71. ^{1}H NMR (300 MHz, DMSO-d_6)[ppm]:7.47(1H, m), 7.76(1H, d, J=6.0 Hz), 7.84-7.95(3H, m), 8.14-8.20(4H, m), 8.22-8.30(6H, m), 8.39(2H, d, J=3.0 Hz), 8.48(2H, m), 8.85(1H, d, J=9.0 Hz), 9.10(1H, s). IR (KBr) [cm^{-1}]: 1592, 1506, 1420, 1381, 1324, 1209, 1141, 1073, 834, 719, 546. ESI-MS(DMSO): m/z 583.1 ($[Ru(phen)_2(salH)]^+$).

Cell culture. The A549, BGC823 MDA-MB-231 cell lines were obtained from the Cell Bank of Type Culture Collection of the Chinese Academy of Sciences (Shanghai, China). The cells were cultured in RPMI-1640 medium (Gibco, Milano, Italy) supplemented with 10 % foetal bovine serum (FBS) (HyClone, Logan, UT, USA), 100 U/mL penicillin and 100 μg/mL streptomycin at 37 ℃ and 5% CO_2. For passaging, the cells were washed with PBS, incubated with trypsin (GIBCO, Invitrogen, UK), and then re-seeded into fresh medium. For seeding, trypsinized and PBS washed cells were counted by microscopy using a Neubauer Haemocytometer (Assistant, Germany), and appropriate numbers of cells were seeded into the plates.

Cytotoxicity assay. The A549, BGC823 and MDA-MB-231 cells were cultured in RPMI-1640 medium (Gibco, Milano, Italy). Standard MTT assay procedures were used. The cells were placed in 96-well microassay culture plates at a density of 3×10^3 cells per well and incubated overnight at 37 ℃ in a 5% CO_2 incubator. The Ru-complexes were prepared as stock solutions of 20 mg/ml in DMSO. The stock solutions of the Ru-complexes were stored at -20 ℃ and diluted with fresh medium to the different final working concentrations (1-150 μM) when needed. The control wells were prepared by adding culture medium containing 0.5% (v/v) DMSO. The plates were incubated at 37 ℃ in a 5% CO_2 incubator for 24 h or 48 h. After the incubation, 10 μl of the MTT dye solution (5 mg/ml) were added to each well. After incubation for 4 h, 200 μl of DMSO was used to solubilize the MTT formazan crystals. The absorbance of each well was measured with a microplate spectrophotometer at a wavelength of 570

nm. The IC_{50} values were determined by plotting the percentage of viable cells against the concentration on a logarithmic graph and determining the concentration at which 50% of the cells remained viable relative to the control. Each experiment was repeated at least three times to obtain the mean values.

Clone formation assay. The cells were plated in 35 mm culture dishes at 2,000 cells per dish and incubated overnight at 37 ℃ in a 5% CO_2 incubator. Then, the drugs were added to the plates at pre-calculated concentration. The cells were allowed to grow for two weeks before being stained with Crystal Violet (0.5%, m/v). Then, the cells were washed four times with PBS for a total of 20 min and the images were captured. All experiments were repeated at least three times, and similar results were obtained in each trial.

Apoptosis assay using Hoechst 33258 staining. The cancer cells were seeded onto chamber slides in 24-well plates at a density of 2×10^4 cells per well and incubated for 24 h at 37 ℃ in a 5% CO_2 incubator. Then, the medium was removed and replaced with control medium (final DMSO concentration, 0.5% v/v) or experimental media containing the Ru-complexes (5 to 40 μM) and incubated for 24 h. After the incubation, the media were removed, the cells were washed twice with PBS, and then fixed with paraformaldehyde (4%, m/v). The cell nuclei were counterstained with Hoechst 33258 (2 μg/ml in PBS) for 5 min. Then, the slides were observed and imaged by a laser scanning con-focal microscope, with excitation at 350 nm and emission at 460 nm.

Fluorescence titration. The fluorescence spectra of the titrations were measured using a Perkin-Elmer LS-55 spectrometer (Perkin-Elmer, USA) with Ex/Em slits at 10 nm/10 nm. Fluorescence decay was performed using freshly diluted Ru-complexes in aqueous solutions with Tris-Cl (10^{-4} M, pH 7.4). The fluorescence titrations were performed at a fixed concentration of the Ru-complexes, 19.6 μM **Ru-1**, 18.1 μM **Ru-2** and 18.3 μM **Ru-3**, with various concentrations of CT-DNA. The fluorescence from 500 to 700 nm was recorded with an Ex of 450 nm.

5-ethynyl-2'-deoxyuridine incorporation assay. The A549, BGC823 and MDA-MB-231 cells were seeded in 24-well plates at a density of 5×10^4 per well and incubated for 24 h at 37 ℃ in a 5% CO_2 incubator. Then, the medium was removed and replaced with control medium (final DMSO concentration, 0.5% v/v) or experimental media containing the Ru-complexes (5 to 40 μM). After incubation for 24 h, 5-ethynyl-2'-deoxyuridine (EdU) (Cell light EdU DNA imaging kit, RiboBio, Guangzhou, China) was added and the cells were incubated for an additional 2 h. After incubation, the EdU media mixtures were removed and the cells were fixed with paraformaldehyde (4%, m/v) for 20 min at room temperature. Then,

the cells were washed with glycine (2 mg/ml) for 5 min in a shaker and incubated with PBST (PBS buffer with 0.5% Trion X-100) for 10 min. After washing twice with PBS, the cells were stained with click reaction buffer (Tris–Cl, pH 8.5, 100 mM; $CuSO_4$, 1 mM; Apollo 550 fluorescent azide, 100 mM; and ascorbic acid, 100 mM) for 30 min in the dark. Then, the cells were washed with 0.5% PBST three times, stained with Hoechst 33258 (5 μg/ml) for 10 min at room temperature, and finally washed with 0.5% PBST five times. Representative images were captured and analyzed using a fluorescence microscope.

JC-1 staining. The loss of mitochondrial membrane potential (ΔΨm) was assessed by 5, 5′, 6,6′-tetrachloro-1, 1′, 3,3′-tetraethylbenzimidazole-carbocyanide iodine (Beyotime, Shanghai, China) staining using a fluorescence microscope (IX71, Olympus). The BGC823 cells were seeded into 12-well plates at a density of 1×10^5 per well and incubated for 12 h at 37 ℃ in a 5% CO_2 incubator. Then, the cells were incubated with 5 μM CDDP and **Ru-2** for 12 h, followed by JC-1 staining for 20 min at 37 ℃. The cells on the chamber slides were scanned with a fluorescence microscope. JC-1 can aggregate in normal mitochondria and exhibit red fluorescence, while the monomeric form of JC-1 is present in the cytosol and exhibits green fluorescence. The dissipation of ΔΨm could be shown as increased green fluorescence, and the ratio of red and green fluorescence was used to evaluate apoptosis[70].

Apoptosis assay by flow cytometry. Cell apoptosis was assessed by flow cytometry using the Annexin V-FITC/PI Apoptosis Detection Kit (BD, New York, USA). The BGC823 cells were seeded into 6-well plates at a density of 2×10^5 cells per well and incubated with 5 μM CDDP or 5 and 10 μM **Ru-2** for 24 h. The cells were harvested, centrifuged for 5 min at 200×g and 4 °C, and the supernatant was discarded. Then, the cells were resuspended in 100 μl of Annexin V Binding Buffer, and 5 μl of Annexin V and 10 μl of PI were added to each tube. After incubation for 15 minute in the dark at room temperature, 400 μl of ice-cold Annexin V Binding Buffer was added to each tube. The samples were analysed by flow cytometry at 527 and 586 nm using 488 nm as the excitation wavelength.

Nude mice xenograft Model in vivo. Athymic nude mice were purchased from Hunan Slac-Jinda Laboratory Animal Co., Ltd (Hunan, China), and the experimental protocols were approved by the Experimental Animal Center of Wuhan University. All animals were 6-7 weeks of age at the time of injection. Approximately 2×10^7 cells were subcutaneously implanted into the right flank of the mice. The tumour volumes were calculated as an ellipsoid volume using the formula $(\pi/6)lw^2$, where l = the larger measurement and w = the smaller measurement. When the volume of tumours reached ~100 mm^3, the mice were randomly distributed into three groups (n=6). The vehicle group received with normal

saline, the treatment groups were given 4 mg/kg body weight CDDP or 5 mg/kg body weight **Ru-2**, every other day for 30 days. During treatment, the body weights and tumour volumes were recorded every three days. For pathological examination, tissue sections were fixed in formalin, embedded in paraffin blocks, and stained with haematoxylin and eosin (H&E). Blood samples from the nude mice were subjected to an analysis of the serum ALT and AST activities, according to the method from the serum ALT or AST assay kits (Nanjing Jiancheng Bioengineering Institute, Nanjing, China).

Statistical Analysis. Unless indicated otherwise, the results are presented as the means ± SD. The differences between the different treatments were analysed using the two-sided Student's t test. P values less than 0.05 were considered significant.

Acknowledgements

We thank Gerard Rushworth for the correction of grammatical errors and the critical reading of the manuscript. This work was financially supported by the National Natural Science Foundation of China (NSFC, grant no. 31570353, 31170328, 81572943) and the Fundamental Research Funds for the Central Universities (No. 2014301020203).

Notes and references

1. I. Kostova, *Curr Med Chem*, 2006, **13**, 1085-1107.
2. R. Siegel, D. Naishadham and A. Jemal, *CA Cancer J Clin*, 2013, **63**, 11-30.
3. S. Kala, A. S. Mak, X. Liu, P. Posocco, S. Pricl, L. Peng and A. S. Wong, *J Med Chem*, 2014, **57**, 2634-2642.
4. P. J. DiSaia and J. D. Bloss, *Gynecol Oncol*, 2003, **90**, S24-32.
5. B. Rosenberg, L. VanCamp, J. E. Trosko and V. H. Mansour, *Nature*, 1969, **222**, 385-386.
6. J. Lu, Q. Sun, J. L. Li, L. Jiang, W. Gu, X. Liu, J. L. Tian and S. P. Yan, *J Inorg Biochem*, 2014, **137**, 46-56.
7. G. Y. Li, K. J. Du, J. Q. Wang, J. W. Liang, J. F. Kou, X. J. Hou, L. N. Ji and H. Chao, *J Inorg Biochem*, 2013, **119**, 43-53.
8. O. Pinato, C. Musetti, N. P. Farrell and C. Sissi, *J Inorg Biochem*, 2013, **122**, 27-37.
9. L. Kelland, *Nat Rev Cancer*, 2007, **7**, 573-584.
10. P. J. Loehrer and L. H. Einhorn, *Ann Intern Med*, 1984, **100**, 704-713.
11. A. S. Abu-Surrah, *Mini Rev Med Chem*, 2007, **7**, 203-211.
12. K. Wiglusz and L. Trynda-Lemiesz, *J Photoch Photobio A*, 2014, **289**, 1-6.
13. A. A. Argyriou, P. Polychronopoulos, G. Iconomou, E. Chroni and H. P. Kalofonos, *Cancer Treat Rev*, 2008, **34**, 368-377.
14. J. T. Hartmann and H. P. Lipp, *Expert Opin Pharmacother*, 2003, **4**, 889-901.
15. C. Gong, L. Qian, H. Yang, L. L. Ji, H. Wei, W. B. Zhou, C. Qi and C. H. Wang, *BMC Complement Altern Med*, 2015, **15**, 283.
16. A. Zahedi, M. Nematbakhsh, M. Moeini and A. Talebi, *J Nephropathol*, 2015, **4**, 134-140.

17. T. Karasawa and P. S. Steyger, *Toxicol Lett*, 2015, **237**, 219-227.
18. A. Avan, T. J. Postma, C. Ceresa, A. Avan, G. Cavaletti, E. Giovannetti and G. J. Peters, *Oncologist*, 2015, **20**, 411-432.
19. S. R. McWhinney, R. M. Goldberg and H. L. McLeod, *Mol Cancer Ther*, 2009, **8**, 10-16.
20. M. Schrader, M. Muller, B. Straub and K. Miller, *Reprod Toxicol*, 2001, **15**, 611-617.
21. S. J. Howell and S. M. Shalet, *J Natl Cancer Inst Monogr*, 2005, DOI: 10.1093/jncimonographs/lgi003, 12-17.
22. S. O'Grady, S. P. Finn, S. Cuffe, D. J. Richard, K. J. O'Byrne and M. P. Barr, *Cancer Treat Rev*, 2014, **40**, 1161-1170.
23. M. C. Rose, E. Kostyanovskaya and R. S. Huang, *Genomics Proteomics Bioinformatics*, 2014, **12**, 198-209.
24. A. Stenzel-Bembenek, D. Sagan, M. Guz and A. Stepulak, *Postepy Hig Med Dosw (Online)*, 2014, **68**, 1361-1373.
25. S. Chatterjee, A. E. Norton, M. K. Edwards, J. M. Peterson, S. D. Taylor, S. A. Bryan, A. Andersen, N. Govind, T. E. Albrecht-Schmitt, W. B. Connick and T. G. Levitskaia, *Inorg Chem*, 2015, **54**, 9914-9923.
26. B. A. Iglesias, J. F. Barata, P. M. Pereira, H. Girao, R. Fernandes, J. P. Tome, M. G. Neves and J. A. Cavaleiro, *J Inorg Biochem*, 2015, **153**, 32-41.
27. X. Xue, M. D. Hall, Q. Zhang, P. C. Wang, M. M. Gottesman and X. J. Liang, *ACS Nano*, 2013, **7**, 10452-10464.
28. H. S. Oberoi, N. V. Nukolova, A. V. Kabanov and T. K. Bronich, *Adv Drug Deliv Rev*, 2013, **65**, 1667-1685.
29. T. S. Morais, F. Santos, L. Corte-Real, F. Marques, M. P. Robalo, P. J. Madeira and M. H. Garcia, *J Inorg Biochem*, 2013, **122**, 8-17.
30. G. B. Jiang, Y. Y. Xie, G. J. Lin, H. L. Huang, Z. H. Liang and Y. J. Liu, *J Photochem Photobiol B*, 2013, **129**, 48-56.
31. Y. J. Liu, C. H. Zeng, Z. H. Liang, J. H. Yao, H. L. Huang, Z. Z. Li and F. H. Wu, *Eur J Med Chem*, 2010, **45**, 3087-3095.
32. L. Xu, N. J. Zhong, H. L. Huang, Z. H. Liang, Z. Z. Li and Y. J. Liu, *Nucleosides Nucleotides Nucleic Acids*, 2012, **31**, 575-591.
33. Y. J. Liu, Z. H. Liang, Z. Z. Li, J. H. Yao and H. L. Huang, *DNA Cell Biol*, 2011, **30**, 829-838.
34. P. Jaividhya, R. Dhivya, M. A. Akbarsha and M. Palaniandavar, *J Inorg Biochem*, 2012, **114**, 94-105.
35. V. M. Manikandamathavan and B. Unni Nair, *Eur J Med Chem*, 2013, **68**, 244-252.
36. E. C. Constable, S. Decurtins, C. E. Housecroft, T. D. Keene, C. G. Palivan, J. R. Price and J. A. Zampese, *Dalton Trans*, 2010, **39**, 2337-2343.
37. C. A. Wootton, C. Sanchez-Cano, H. K. Liu, M. P. Barrow, P. J. Sadler and P. B. O'Connor, *Dalton Trans*, 2015, **44**, 3624-3632.
38. L. K. Filak, D. S. Kalinowski, T. J. Bauer, D. R. Richardson and V. B. Arion, *Inorg Chem*, 2014, **53**, 6934-6943.
39. G. Sava and A. Bergamo, *Int J Oncol*, 2000, **17**, 353-365.
40. J. M. Rademaker-Lakhai, D. van den Bongard, D. Pluim, J. H. Beijnen and J. H. Schellens, *Clin Cancer Res*, 2004, **10**, 3717-3727.
41. Y. Zhang, L. Lai, P. Cai, G. Z. Cheng, X. M. Xu and Y. Liu, *New J Chem*, 2015, **39**, 5805-5812.
42. Y. Zhang, P. C. Hu, P. Cai, F. Yang and G. Z. Cheng, *Rsc Advances*, 2015, **5**, 11591-11598.
43. P. Martinez-Bulit, A. Garza-Ortiz, E. Mijangos, L. Barron-Sosa, F. Sanchez-Bartez, I. Gracia-Mora, A. Flores-Parra, R. Contreras, J. Reedijk and N. Barba-Behrens, *J Inorg Biochem*, 2015, **142**, 1-7.
44. A. Srishailam, Y. Kumar, P. Reddy, N. Nambigari, U. Vuruputuri, S. Singh and S. Satyanarayana, *Journal of Photochemistry and Photobiology B-biology*, 2014, **132**, 111-123.
45. S. Karki, S. Thota, S. Darj, J. Balzarini and E. De Clercq, *Bioorg Med Chem*, 2007, **15**, 6632-6641.
46. A. Garzaortiz, P. Maheswari, M. Lutz, M. Siegler and J. Reedijk, *Journal of Biological Inorganic Chemistry*, 2014, **19**, 675-689.
47. J. U. Ahmad, M. T. Raisanen, M. Nieger, M. Leskela and T. Repo, *Inorg Chim Acta*, 2012, **384**, 275-280.
48. L. Hajikhanmirzaei, E. Safaei, A. Wojtczak and Z. Jaglicic, *Inorg Chim Acta*, 2015, **430**, 125-131.
49. S. Wu and S. Lu, *Journal of Molecular Catalysis A-chemical*, 2003, **198**, 29-38.

50. J. Ahmad, M. Raisanen, M. Nieger, M. Leskela and T. Repo, *Inorg Chim Acta*, 2012, **384**, 275-280.
51. M. Xue and S. X. Liu, *Chinese J Inorg Chem*, 2013, **29**, 1319-1327.
52. S. Pal,*Z Anorg Allg Chem*, 2002, **628**, 2091-2098.
53. E. C. Constable, C. E. Housecroft, P. Kopecky, C. J. Martin, I. A. Wright and J. A. Zampese, *Polyhedron*, 2013, **64**, 38-44.
54. S. Pal and S. Pal, *Inorg Chem*, 2001, **40**, 4807-4810.
55. S. Pal, D. Bandyopadhyay, D. Datta and A. Chakravorty, *J Chem Soc Dalton*, 1985.
56. J. F. Li, R. Z. Huang, G. Y. Yao, M. Y. Ye, H. S. Wang, Y. M. Pan and J. T. Xiao, *Eur J Med Chem*, 2014, **86**, 175-188.
57. S. Feng, S. Cong, X. Zhang, X. Bao, W. Wang, H. Li, Z. Wang, G. Wang, J. Xu, B. Du, D. Qu, W. Xiong, M. Yin, X. Ren, F. Wang, J. He and B. Zhang, *Nucleic Acids Res*, 2011, **39**, 6669-6678.
58. S. Banerjee, J. A. Kitchen, T. Gunnlaugsson and J. M. Kelly, *Org Biomol Chem*, 2013, **11**, 5642-5655.
59. S. Banerjee, S. A. Bright, J. A. Smith, J. Burgeat, M. Martinez-Calvo, D. C. Williams, J. M. Kelly and T. Gunnlaugsson, *J Org Chem*, 2014, **79**, 9272-9283.
60. V. G. Vaidyanathan and B. U. Nair, *J Inorg Biochem*, 2003, **94**, 121-126.
61. J. M. Kelly, D. J. Mcconnell, C. Ohuigin, A. B. Tossi, A. Kirschdemesmaeker, A. Masschelein and J. Nasielski, *J Chem Soc Chem Comm*, 1987, DOI: Doi 10.1039/C39870001821, 1821-1823.
62. A. Kirschdemesmaeker, G. Orellana, J. K. Barton and N. J. Turro, *Photochem Photobiol*, 1990, **52**, 461-472.
63. S. F. Zhang, B. P. Ling, F. L. Qu and X. J. Sun, *Spectrochim Acta A*, 2012, **97**, 521-525.
64. I. U. H. Bhat and S. Tabassum, *Spectrochim Acta A*, 2009, **72**, 1026-1033.
65. N. Shahabadi, S. Kashanian and F. Darabi, *Eur J Med Chem*, 2010, **45**, 4239-4245.
66. S. Tabassum, I. U. H. Bhat and F. Arjmand, *Spectrochim Acta A,* 2009, **74**, 1152-1159.
67. N. Shahabadi, S. Kashanian and F. Darabi, *DNA Cell Biol*, 2009, **28**, 589-596.
68. C. Balague, J. Zhou, Y. Dai, R. Alemany, S. F. Josephs, G. Andreason, M. Hariharan, E. Sethi, E. Prokopenko, H. Y. Jan, Y. C. Lou, D. Hubert-Leslie, L. Ruiz and W. W. Zhang, *Blood*, 2000, **95**, 820-828.
69. Y. Lu and A. I. Cederbaum, *Toxicol Sci*, 2006, **89**, 515-523.
70. H. Xin, X. H. Liu and Y. Z. Zhu, *Eur J Pharmacol*, 2009, **612**, 75-79.

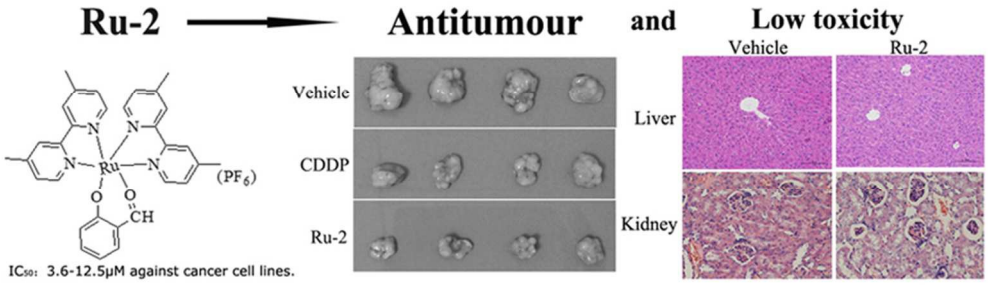

77x22mm (300 x 300 DPI)